JMEPEG
https://doi.org/10.1007/s11665-024-10076-7

1059-9495/$19.00

ORIGINAL RESEARCH ARTICLE

Changing Mechanisms of High-Temperature Oxidation of Zr-1%Nb Alloy in Air and Steam by Surface Modification with Charged Particles

Mikhail Slobodyan, Konstantin Ivanov, Vasiliy Klimenov, Irina Strelkova, Vladislav Tarbokov, Sergey Pavlov, Gennady Remnev, Maxim Elkin, and Vladimir Uglov

Submitted: 19 March 2024 / Revised: 16 July 2024 / Accepted: 18 July 2024

The Zr-1%Nb alloy is widely used as a structural material for nuclear fuel assemblies of light water reactors. One of its key properties is the behavior upon a possible loss-of-coolant accident (LOCA) that can be changed by the surface modification procedures. This paper presents the research results on the effects of both high-intense pulsed ion beam (HIPIB) irradiation and high-current pulsed electron beam (HCPEB) processing on the kinetics of its oxidation at 1200 °C in air and steam, similar to the LOCA conditions. HIPIB irradiation led to more uniform reliefs on the sample surfaces but did not change their phase composition. However, both *a* and *c* lattice parameters decreased slightly with a simultaneous increase in microstrains. After HCPEB processing, the general patterns of changes in the modified surface layers were similar, but microcracks were found in some areas. In all studied cases, weight gains were greater after oxidation in air than those in steam. Nevertheless, diffusion of oxygen and the formation of scales occurred more slowly in the modified surface layers due to their distorted crystal lattices. The main reason for the variations was different physical processes that had occurred when the surfaces had been modified with charged ions and electrons.

Keywords high-intense pulsed ion beam (HIPIB), high-current pulsed electron beam (HCPEB), high-temperature oxidation, surface modification, zirconium alloy

1. Introduction

Since the 1940s, zirconium alloys are key structural materials for nuclear fuel assemblies of light water reactors (Ref 1). Under normal operating conditions, claddings, space grids and other parts from zirconium alloys are exposed to radiation, high temperatures and other aggressive factors. In addition, they may be oxidized at high temperatures (up to 1204 °C) in environments containing various steam concentrations during possible loss-of-coolant accidents (LOCAs) (Ref 2). In such cases, an emergency system operates and the nuclear reactor core is cooled with water. As a result, fuel claddings can collapse due to embrittlement of the metal. This issue has become extremely urgent after the Fukushima Daiichi accident in 2011 (Ref 3). In this regard, numerous studies are ongoing by research groups around the world on the behavior of different zirconium alloys during high-temperature oxidation in various environments (Ref 4-23). It should be noted that this parameter is greatly affected by the surface properties, which are determined by production routs, including chemical etching in many cases. However, this procedure is not environmentally friendly and chemical residues on the treated surfaces impair their functional properties.

Due to the mentioned challenges, significant efforts of worldwide nuclear fuel manufacturers and research teams aimed at optimizing the surface treatment procedures for claddings made of zirconium alloys. This fact is fully consistent with the accident tolerant fuel (ATF) concept for light water reactors (Ref 24), which includes deposition of coatings (Ref 25) and/or high-energy surface processing (Ref 26), enabling to protect nuclear fuel assembles upon possible LOCAs. In the first case, it is assumed that coatings from chromium, ceramics, composites or heat-resistant alloys should be both thermal and diffusion barriers, shielding the base metal from oxidation and hydrogenation by steam at a temperature of about 1200 °C. However, many issues should be solved for achieving this goal, such as low adhesion of the coatings, mutual diffusion of their components into the base metal and variations in thermal properties of the coatings and the substrates. In turn, high-energy surface processing makes it possible to modify surface layers, slowing down diffusion of oxygen and hydrogen into the base metal due to the distortion of its crystal lattice. Nevertheless, no industrial procedures have been developed and implemented yet, despite a huge number of published papers in this area, summarized in a recent review (Ref 26).

Mikhail Slobodyan, Tomsk Scientific Center of the Siberian Branch of the Russian Academy of Sciences, 10/4, Akademicheskii Prospekt, Tomsk, Russia 634055; **Konstantin Ivanov**, Institute of Strength Physics and Materials Science SB RAS, 2/4, Akademicheskii Prospekt, Tomsk, Russia 634055; **Vasiliy Klimenov, Irina Strelkova, Vladislav Tarbokov, Sergey Pavlov,** and **Gennady Remnev**, Tomsk Polytechnic University, 30, Lenin Prospekt, Tomsk, Russia 634050; **Maxim Elkin**, Tomsk Polytechnic University, 30, Lenin Prospekt, Tomsk, Russia 634050; and 'Polyus' Research and Production Center, 56v, Kirov Prospekt, Tomsk, Russia 634050; and **Vladimir Uglov**, Belarusian State University, 4, Nezavisimosti Prospekt, 220030 Minsk, Belarus. Contact e-mail: sms.msc@yandex.ru.

Published online: 17 September 2024

One of the high-energy surface processing methods is irradiation with high-intense pulsed ion beams (HIPIBs) that is trying to be implemented for a wide range of metals, steels and alloys (Ref 27-39). As a result, their functional properties have been improved in some cases. As an instance, corrosion resistance has been enhanced for the AZ31 magnesium alloy (Ref 30, 34) and austenitic stainless steels (Ref 28, 39). Also, HIPIB irradiation has been proposed to extend the durability of nuclear fuel claddings (Ref 26), since no blisters have been observed on the modified surfaces of samples from the Zr-1%Nb alloy (one of the most widely used in light water reactors) after their oxidation at 1200 °C in steam for 60 secs (Ref 37) (in contrast to the as-received cold-rolled specimens). In addition, some other techniques have been considered promising for this purpose (Ref 26), including high-current pulsed electron beam (HCPEB) processing. For example (Ref 40), it has enabled to slow down weight gain rates upon oxidation of the Zr-1%Nb alloy under conditions, similar to those described in the second section. It should be noted that no patterns of implementation of these high-energy surface processing methods have not been compared so far, despite a fairly detailed analysis of the physical processes taking place (Ref 41).

Based on the above, the aim of this study was to assess the effects of both HIPIB irradiation and HCPEB processing of the Zr-1%Nb alloy on the kinetics and mechanisms of its oxidation at 1200 °C in air and steam. The obtained results were compared with each other and with previously reported data. Both similarities and differences of these patterns were discussed, as well as future research directions were suggested.

2. Materials and Methods

Plates with dimensions of 15 × 5 × 0.5 mm from the Zr-1%Nb alloy (the E110 grade according to the Russian classification) were used as samples (similar to (Ref 37, 40)). Initially, their both surfaces were grinded sequentially with sandpapers of 600, 800, 1000 and 2000 grit sizes to obtain the *Ra* roughness of ~ 100 nm. Then, they were cleaned and degreased immediately before high-energy processing.

HIPIB irradiation was performed using the 'TEMP-4' accelerator (Ref 29, 36, 37, 39). The sample edges were not irradiated additionally. The following parameters were applied on the basis of the previous experience of the authors (Ref 36-39): an accelerated voltage of 160-180 keV, a pulse duration of 100 ns and an ion current density on a target of 110-120 A/cm^2. The beam was composed of carbon ions (~70%) and protons (~30%). The energy density at the target, measured by the thermal imaging method (Ref 42), was ~ 2 J/cm^2 per pulse. The number of pulses was three for each side. Pressure in a chamber was about $2.67 \cdot 10^{-2}$ Pa.

HCPEB processing of both surfaces of the samples was carried out using a 'RITM-IZ' installation under the optimal conditions determined in the trial study by the authors (Ref 40). The following parameters were applied: an accelerating voltage of 30 kV, an energy density of 5 J/cm^2, a pulse duration of 2 μs and the number of pulses of 10 for both sides. Argon pressure in a chamber was about $5 \cdot 10^{-2}$ Pa. Under these conditions, surface layers several microns thick were modified without phase transformations and/or deep cracking (Ref 40).

Changes in the modified layers were assessed using the method, previously implemented in (Ref 43). The surface layers were examined by x-ray diffraction analysis with an 'Ultima IV' diffractometer (Rigaku, Japan) in parallel beam geometry using copper radiation (0.154179 nm). An 'NT-MDT Integra Prima' atomic force microscope was used for measuring roughness at a 100 μm base.

As in the previous investigations by the authors (Ref 37, 40), high-temperature oxidation was carried out with an 'ITM' facility at a temperature of 1200 ± 3 °C in air and steam for 30, 60 and 180 secs. Its detailed description was reported in (Ref 37). Weight changes were determined by weighing the samples using a 'RADWAG MXA-21' scales with a maximum error of ± 0.01 mg. Three samples were tested for each combination of the surface characteristics and the oxidation conditions. The weight gain values were statistically processed by applying the $Y = B \cdot ln(X) + A$ logarithmic fit.

The sample surfaces were examined using a 'Carl Zeiss EVO 50' scanning electron microscope (SEM) at an accelerated voltage of 20 kV, equipped with a back scattered electron (BSE) detector. An energy-dispersive spectroscopy (EDS) analysis was carried out with a 'JEOL JSM-6000PLUS' SEM. For metallographic examinations, the samples were prepared using standard methods similarly to (Ref 37, 40), which included grinding with the above-mentioned sandpapers and final polishing on a cloth with an aqueous chromium oxide suspension. The sample cross sections were investigated with an 'Axio Observer A1m' optical microscope.

3. Results

3.1 Surface Modification

Figure 1 shows SEM images of the surfaces on the studied samples. On the as-received cold-rolled samples (Fig. 1a), some scratches, discontinuities and inclusions were observed. According to the results of the EDS analysis (Fig. 2), such inclusions were complex oxycarbonitride compounds. After HIPIB irradiation, no shallow scratches were found while deeper discontinuities possessed smoother reliefs (Fig. 1b). The *Ra* roughness on the sample surfaces decreased down to 50-60 nm, which was only half of the initial level of ~ 100 nm. In addition to the initial inclusions, new black ones were observed, characterized by dimensions within 1 μm (visible only at a high magnification). They could be complex oxycarbonitride compounds (according to Fig. 2) and include zirconium hydrides (Ref 44-47), since the beam composition had consisted of both carbon ions and protons. In this research, clarification of the chemical composition of these new microinclusions was not carried out due to the lack of their influence on the key findings (discussed below). During HIPIB irradiation, some craters had been formed on the modified surfaces, which were typical for such cases (Ref 26, 48). After HCPEB processing, the sample surfaces (Fig.1c) were characterized by more uniform reliefs (in comparison with the as-received one shown in Fig.1a) and few craters with slightly different morphology due to various mechanisms of their formation (Ref 49), discussed below. More detailed information about the influence of the HCPEB processing parameters on the characteristics of the modified layer on the samples from the Zr-1%Nb alloy can be found in the previous paper by the authors (Ref 40).

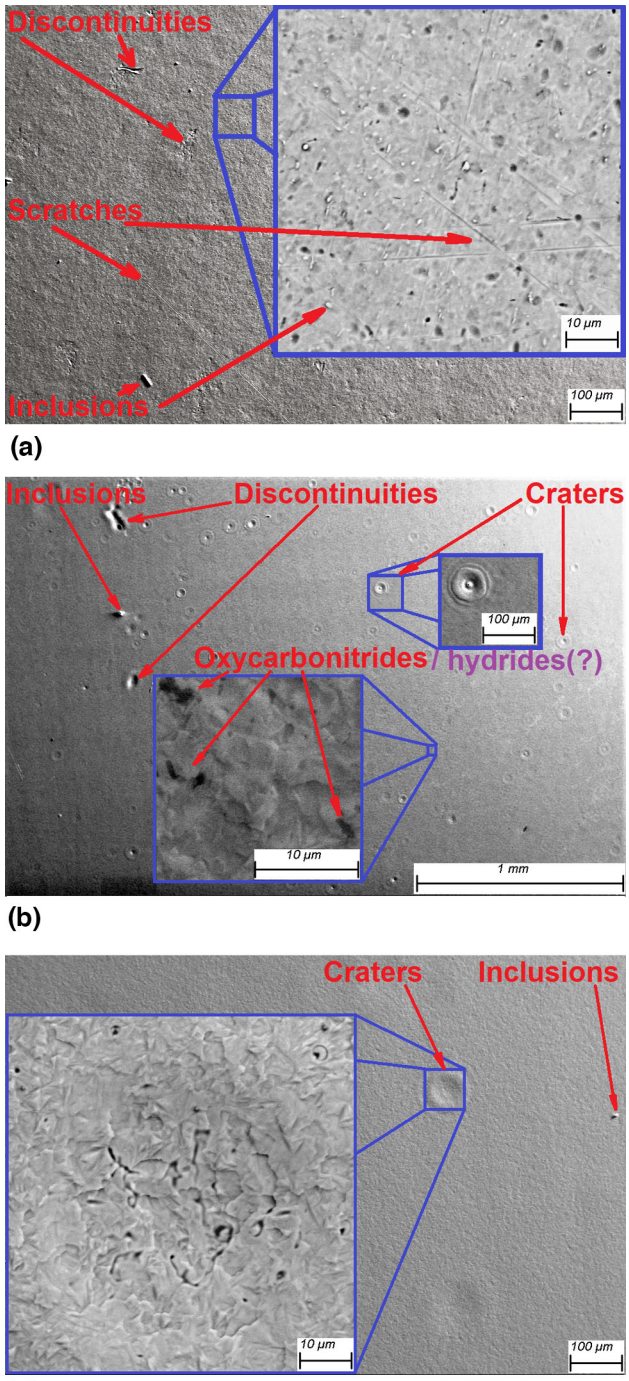

Fig. 1 SEM images of the sample surfaces: (a) as-received, (b) after HIPIB irradiation, (c) after HCPEB processing

Figure 3 and Table 1 show the results of the x-ray diffraction analysis of the surface layers on both as-received sample and one after HIPIB irradiation. In general, the obtained diffraction patterns were as expected, since α-Zr was the main phase (Ref 1). Shifts of the peaks and changes in their shapes also correlated with those previously reported for zirconium alloys irradiated with carbon (Ref 38), helium (Ref 50) and hydrogen (Ref 51) ions, as well as neutrons (Ref 52). For the as-received sample, the diffraction peaks corresponding to the (002) plane of zirconium were more intense compared to others, similarly reported for Zircaloy-4 (Ref 50, 52) and the M5® alloy (Ref 52). In the modified layers, the shifts of the peaks and the changes in their shapes were explained by the radiation-induced distortions of the crystal lattices (Ref 50, 52), which depended on the fluences (doses) and some other nuances (Ref 38, 50-52). This phenomenon was confirmed in this study, according to the data presented in Table 1. In the as-received Zr-1%Nb alloy, the lattice parameters exceeded those for pure zirconium (a = 0.3231 nm; c = 0.5148 nm) due to the presence of niobium as an alloying element. HIPIB irradiation did not change the initial phase composition, but both a and c lattice parameters decreased slightly with enhancing microstrains in the modified layer.

3.2 High-Temperature Oxidation

After high-temperature oxidation, the samples looked about the same. (A typical general view is shown in Fig. 4.) Nevertheless, the oxidation kinetics varied depending on the surface parameters and the test environments. Figure 5 presents the 'weight gain vs oxidation duration' curves for the as-received samples, as well as ones after HIBIP irradiation and HCPEB processing. In all studied cases, two patterns were revealed: 1) The oxidation rates were lower in the 'as-received → HCPEB-processed → HIBIP-irradiated' sequence, and 2) they were greater in air than in steam. These facts were confirmed by variations in the thickness ratios of three layers (oxide, α-Zr(O) and prior-β) after high-temperature oxidation. (Typical cross sections of the oxidized samples are shown in Fig. 6.) Some dispersions in the obtained values were determined by the specifics of the applied test method (Ref 2), as well as their dependence on many factors including the oxidation instability on the sample edges in some cases (Fig.7). However, the purpose of these preliminary studies was to obtain general data on the possibility of improving resistance to high-temperature oxidation for zirconium alloys by high-energy surface processing procedures, but not to report any specific constants. Therefore, in order to assess the reliability of the presented patterns and understand their causes, detailed studies of the dynamics of changes in the morphology of the oxide layers were carried out using their SEM images for all investigated cases. It should be noted that the chemical and phase compositions of the oxide layers were not examined in this study. Nevertheless, previous experiments by the authors under similar conditions (Ref 37) showed the presence of both carbon and nitrogen atoms absorbed from the environment during high-temperature oxidation. Their concentrations varied along the depth, reaching the maximum values of 19.7 and 4.3%, respectively. Given the extremely high reactivity of zirconium and its alloys (Ref 1), this fact contributed to the formation of complex oxycarbonitride compounds inside the formed scales (Ref 44).

Figure 8 shows the dynamics of changes in the surface reliefs of the samples with increasing the duration of high-temperature oxidation. Their variations greatly correlated with the kinetic curves shown in Fig. 5. Upon testing the as-received samples in air (Fig. 8a), initial local discontinuities on their surfaces (Fig. 1a) had been concentrators of pitting accelerated oxidation from the very beginning of the process (the first control point of 30 secs). During this period, many small blisters had formed in some areas of the oxide layers. With prolonging the test duration, they had enlarged, cracked and peeled off in some cases. This fact was undoubtedly the reason

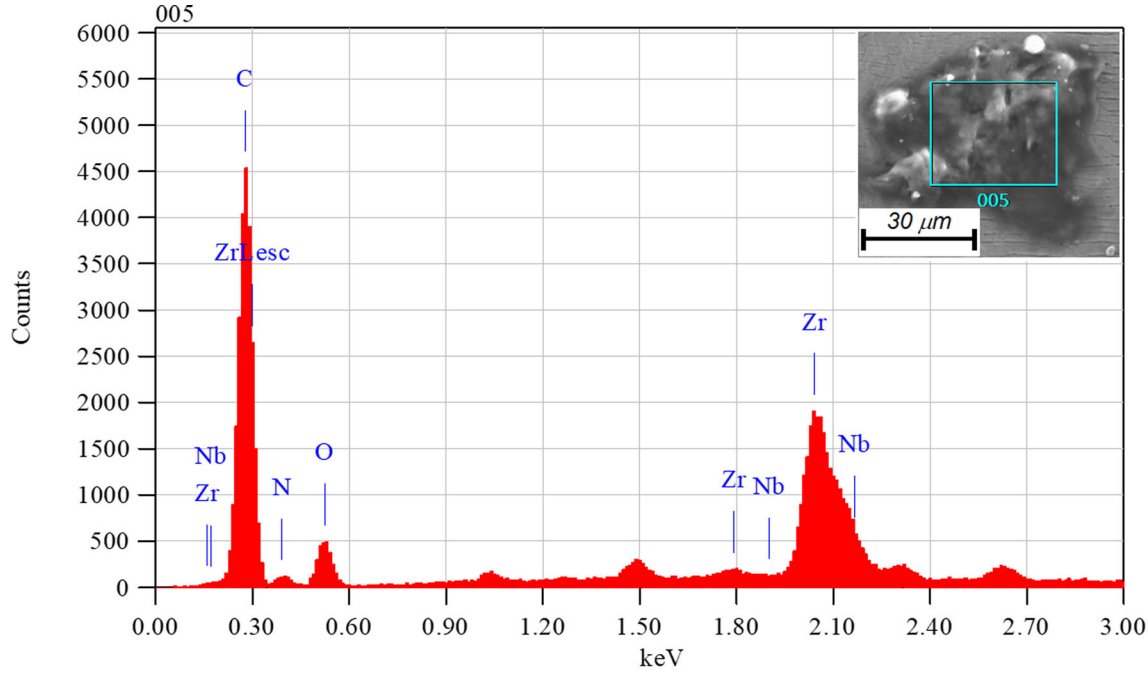

Element	(keV)	Mass%	Sigma	Atom%	Compound	Mass%	Cation	K
C K	0.277	31.31	0.17	54.41				4.6562
N K	0.392	11.51	0.29	17.15				4.2090
O K	0.525	14.28	0.19	18.63				4.8518
Zr L	2.042	42.44	0.14	9.71				85.3055
Nb L*	2.166	0.46	0.08	0.10				0.9775
Total		100.00		100.00				

Fig. 2 Results of the EDS analysis of a typical inclusion on the sample surfaces shown in Figure 1

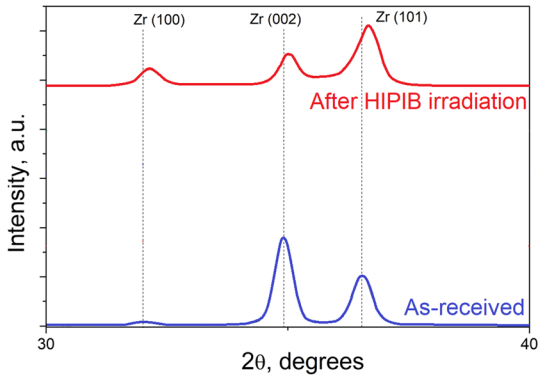

Fig. 3 X-ray diffraction patterns of the as-received sample and one after HIPIB irradiation

for accelerated oxygen diffusion and weight gains for the as-received samples. After varying the test environment from air to steam, the surface character of the oxide layer significantly changed. As in the previous case, initial local discontinuities had been concentrators of pitting accelerated oxidation from the very beginning of the tests. However, the surfaces of all oxidized samples were much more uniform. The formation of

Table 1 Lattice parameters and microstrains in the surface layers of the samples from the Zr-1%Nb alloy

Samples	Lattice parameters		Microstrains, %
	a, nm	*c*, nm	
As-received	0.3239	0.5149	0.23
After HIPIB irradiation	0.3226	0.5136	0.31

Fig. 4 A typical image of the oxidized samples (as-received, air, 180 secs)

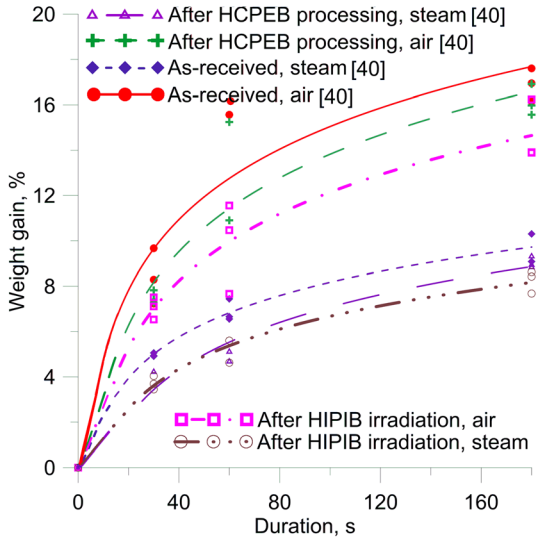

Fig. 5 Oxidation kinetics for the as-received samples, as well as ones after HIBIP irradiation and HCPEB processing

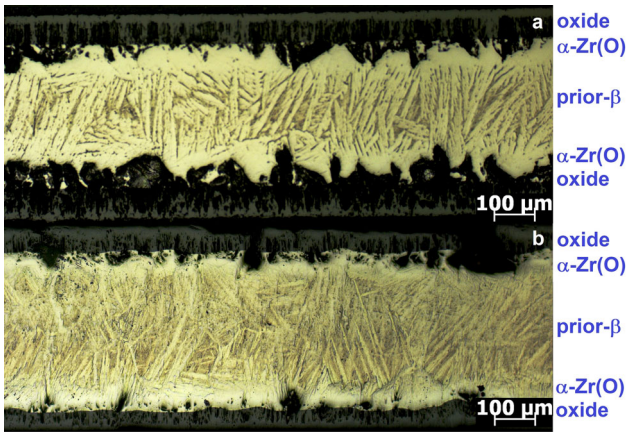

Fig. 6 Typical cross sections of the samples after high-temperature oxidation for 180 secs: (a) as-received, air; (b) after HIPIB irradiation, steam

small blisters was observed only after 180 secs. It should be noted that the oxide layers were without cracks and no peeled off areas were found. As a result, the oxygen diffusion rate and the corresponding weight gain kinetics were lowered (Fig. 5).

After HIPIB irradiation, the oxide layers (Fig. 8b) were significantly different from those on the as-received samples (Fig. 8a) in all studied cases. Since the modified surface layers had been smoothed, concentrators of local pitting oxidation were almost not observed after high-temperature oxidation in air. Craters did not accelerate the oxide layer degradation as well. In general, all modified surface layers were much more uniform than those on the as-received ones after high-temperature oxidation in air. This fact explained the low weight gain kinetics shown in Fig. 5. After testing in steam, a completely different type of the oxide surfaces was observed (Fig. 8b). In particular, lips-like defects began to form on the sample surfaces after 30 secs, the profiles of which became more pronounced (they 'swelled' and 'opened up') as the test duration increased. In addition, several holes within 1 μm in diameter were observed in some areas. Also, precipitation of white

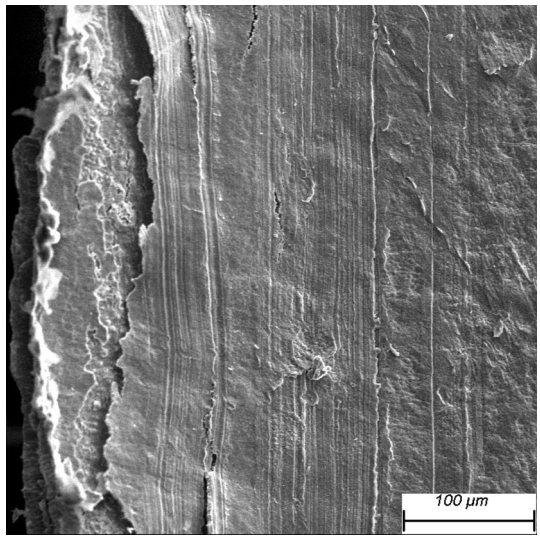

Fig. 7 An example of the non-uniformity of the metal oxidation at the sample edges (as-received, steam, 120 secs)

microinclusions of various intensities was found at the oxidized surfaces. From the one hand, it could be initial black ones (shown in Fig. 1b) that had reacted with steam. From the other hand, similar effect was typical for the breakaway oxidation of the as-received samples from the Zr-1%Nb alloy (Ref 2) that was not observed on the cold-rolled oxidized surfaces in this study (Fig.8a). It should be noted that there is still no generally accepted theory for the mechanism behind nodular oxidation (Ref 2). Despite these features, the slowest weight gain kinetics was obtained upon testing of in steam the samples after HIPIB irradiation (Fig. 5).

HCPEB processing changed the oxidation process as well (Fig.8c). In general, the oxide layers were more uniform than those on the as-received samples after the tests in air (Fig.8a). As after HIPIB irradiation, craters were not pronounced concentrators of local surface damages. However, microcracks were observed at some regions already after 30 secs. Their widths increased with prolonging the test durations. In fact, they were direct channels for oxygen transportation into the metal, which accelerated weight gains for these samples. Also, a small number of large blisters were found in several areas after oxidation for 180 secs. The mentioned differences on the surfaces compared to the previous two cases also explained the reason why the weight gain kinetics was between them in Fig. 5. At a high magnification, the oxide layers looked like a uniform orange peel after oxidation in steam (Fig. 8c). Some separate lips-like defects were observed only after oxidation for 180 secs. It should be noted that the described similarities and differences in the formed oxide layers enabled to identify only general patterns (discussed below). However, further in-depth research is needed to understand their underlying causes.

4. Discussion

4.1 The Effect of Surface Modification

According to the authors, discussion of the obtained results should be started with a brief description of differences between the applied surface modification methods (more detailed

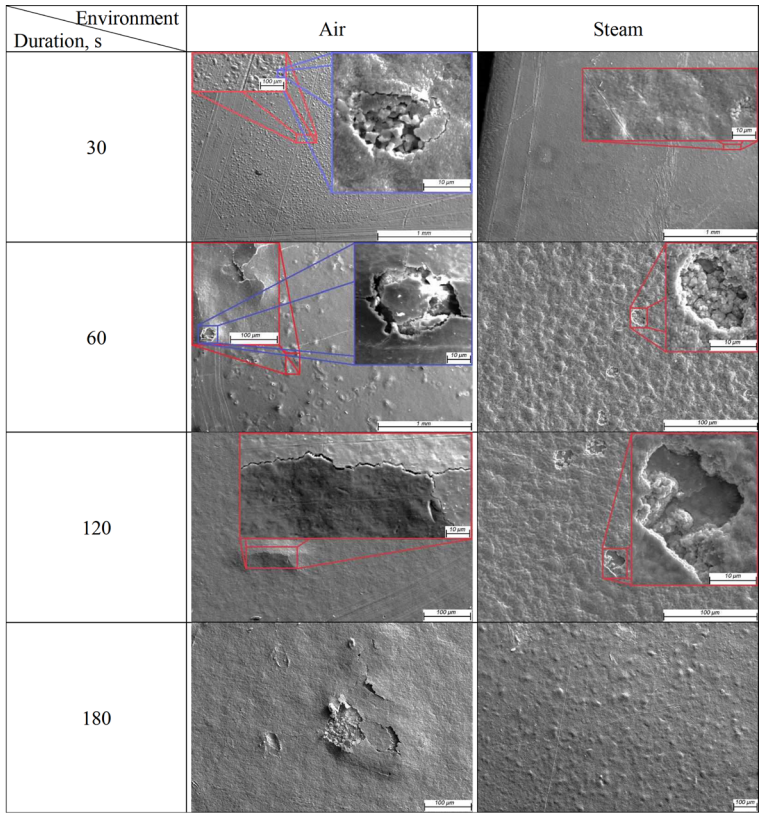

(a)

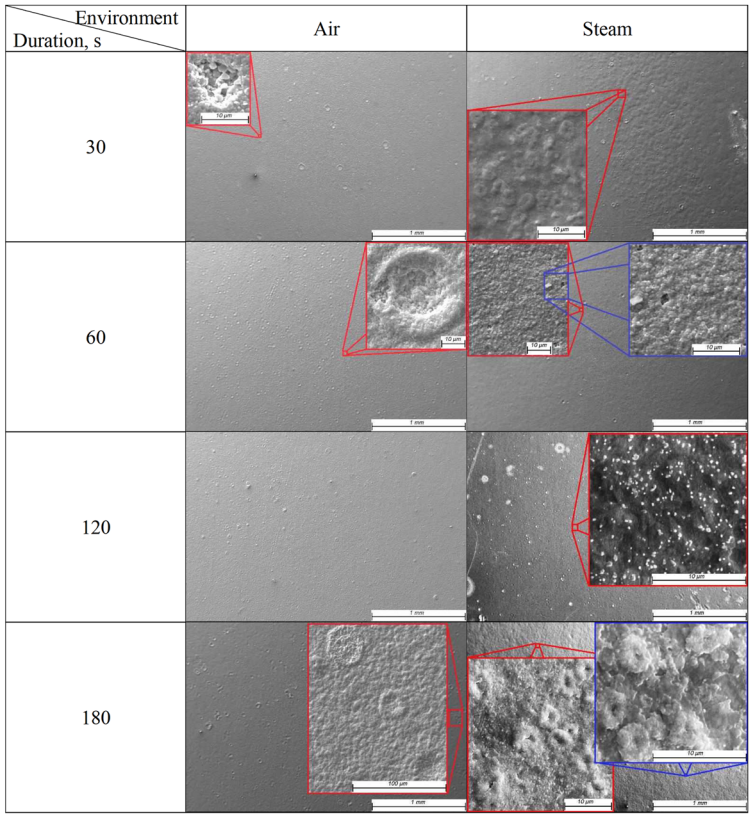

(b)

Fig. 8 SEM images of typical areas of the sample surfaces, characterizing their features depending on both environment and duration of high-temperature oxidation: (a) as-received, (b) after HIPIB irradiation, (c) after HCPEB processing

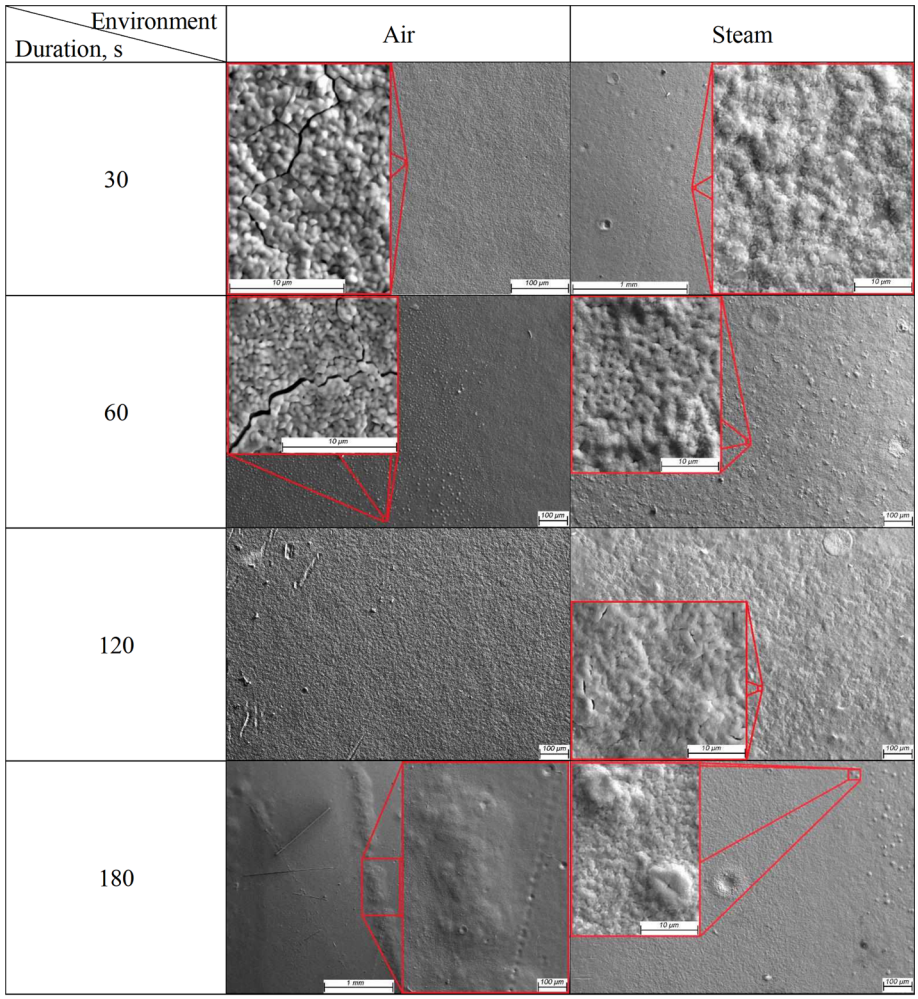

Fig. 8 continued

information can be found in (Ref 41)). Both implemented high-energy surface processing methods were characterized by some common patterns. According to (Ref 41), heating and cooling rates could be about 10^8-10^{11} K/s during HIPIB irradiation, while they lied in a narrower range of $5{\cdot}10^9$-10^{10} K/s upon HCPEB processing. In such cases, spatial temperature gradients reached 10^6-10^7 K/cm and one of the possible channels of energy dissipation was intense movement of atoms in the base metal, depending on the applied parameters and charged particles. In the surface layers, mass transfer was determined mainly by thermal- and pressure-controlled diffusion processes, but shock waves gave the main contribution at great depths. This vortex motion and attenuation of pressure waves during the existence of a liquid phase on the sample surfaces (for several microseconds) could cause significant mixing of the surface layers (which certainly contained initial oxide layers and, probably, some other contaminations in the studied cases). Therefore, an important role in the surface modification processes was played by diffusion in the molten layer and its hydrodynamic mixing among the mechanisms of intensification of atomic migration. However, the stopping ranges differed by orders of magnitude for electrons and ions at the same energies, determining variations of some obtained results (discussed below).

Under the applied HIPIB irradiation parameters, the surface layers of the sample from the Zr-1%Nb alloy were melted and solidified then. However, both heating and cooling rates were (probably) lower than upon HCPEB processing, since the characteristic microreliefs of the modified surfaces ware less pronounced (Fig. 1b and c). This fact was also facilitated by vacuum in the chamber of the HIPIB accelerator in contrast to the argon environment in the second case. Under such conditions, HIPIB irradiation typically resulted in a long-range effect, i.e., a change in the microstructure and properties of metals, steels and alloys at depths significantly exceeding the stopping range of ions (Ref 41). Almost instantaneous heating of the base metal in the surface layers resulted in the generation of thermal stresses in the solid phase (the thermal shock effect), as well as melting and moving of the material from the irradiated surface. The resulting recoil momentum extended compressive forces. Consequently, both processes have a synergistic effect on the irradiated metal. Compared to other types of high-energy surface processing methods, HIPIB irradiation gave the maximum energy input to this effect and formed the most extended surface layers, hardened due to the distortion of the crystal lattice (Ref 41). It should be noted that the cratering mechanism was somewhat different during HIPIB irradiation than that in HCPEB processing. Variations in the

surface tension values of molten inclusions and the matrix contributed to the material flows because of hydrodynamic processes that formed craters on the irradiated surfaces (Ref 48). Then, their profiles developed due to the combined effect of the surface tension variations and their curvatures.

Upon HCPEB processing, high heating and cooling rates of the surface layers, followed by recrystallization processes, formed spatial layers with different types and concentrations of defects. Under the applied conditions, it contributed to melting of a thin surface layer (several micrometers thick), the formation of a heat-affected zone (up to ten micrometers in depth) and a plastic deformation region, characterized by the presence of many dislocations and significant distortions of the crystal lattice to a depth of 50 μm (Ref 26, 40, 41). As a result, the modified surface layers were characterized by great residual stresses. In the surface layer with a thickness of $\sim$ 1 μm, high temperatures and significant thermoelastic stresses acted simultaneously. Therefore, vacancy-type point defects had to be formed due to rapid cooling upon solidification. Additional thermoelastic stresses contributed to the formation of point defects in the crystal lattice, such as clusters of interstitial defects, both screw and edge dislocations. In the heat-affected zone, the microstructure was changed due to the distortion of both grain and dislocation substructures (Ref 41). Respectively, the modified surface layers up to 50 μm thick were characterized by altered conditions for oxygen diffusion and the formation of oxide layers. It should be noted finally that craters were formed by eruption of overheated material volumes in the subsurface layer, characterized by the presence of microinclusions with thermal properties different from those of the base metal (Ref 49). Even at the optimal HCPEB processing parameters (Ref 40), microcracks were found at these areas, while increasing the input energy contributed to their deepening and peeling off of the surface layer. These factors contributed to subsequent cracking of the oxide layers in some regions (Fig.8c) and, accordingly, to the accelerated oxidation rates during the tests (Fig. 5).

As follows from a comparison of the above data with the thicknesses of the oxide layers after high-temperature oxidation (as an example, the HIPIB-irradiated sample in Fig. 6 after testing in steam for 180 secs), their orders were the same. Respectively, diffusion of oxygen and the formation of oxides on the Zr-1%Nb alloy had been mostly in the modified layer with the distorted crystal lattice (Fig. 3, Table 1), which had slowed down these processes. As a result, after HIPIB irradiation, the weight gain curves were the lowest in both air and steam environments. As for HCPEB processing, the slightly higher weight gain curves were observed due to the presence of microcracks and greater residual stresses in the surface layers. It should be noted that HIPIB irradiation with carbon ions and protons had not been the optimal composition for the reactive Zr-1%Nb alloy, since it had easily formed complex compounds with these accelerated particles, lowering resistance to high-temperature oxidation (Ref 2). The reasons for using such beams for HIPIB irradiation were the fact that beams of light ions (hydrogen, carbon, nitrogen, etc.) were easier to generate, and they possessed significantly longer ranges than heavy particles (Ref 41). Nevertheless, this high-energy surface processing method resulted in the slowest weight gain kinetics for all investigation cases. Accordingly, there is a possibility that changing the beam composition with inert argon ions may further improve this characteristic. However, more research is needed to confirm or refute this assumption. In addition, a more detailed study of differences in thin structures of the surface layers should be carried out applying advanced research methods (Ref 41), such as high-resolution transmission electron microscopy, Rutherford backscattering of channeled ions, electron-positron annihilation and secondary ion-mass spectroscopy.

4.2 The Influence of Environmental Humidity

It is known that the effect of the environmental humidity greatly depends on the material being oxidized and the test temperature (Ref 53). Steam molecules could go into chemical reactions with metals, steels and alloys. This phenomenon could reduce ductility of the oxide layers and their peeling. Concerning zirconium and its alloys, very few fragmentary (and contradictory in some cases) data were published so far on this topic (Ref 2, 6, 19, 21, 23, 54-66). The results obtained in the presented research, correlated to some extent with information reported in (Ref 2, 23, 59). The similarities included the facts that the metal degradation process was faster in air than in steam (Ref 2, 23), as well as the proportion of the oxide, α-Zr(O) and prior-β layers (according to Fig. 6) changed similar to that reported in (Ref 59). Both goals and conditions of all other mentioned experiments (Ref 6, 19, 21, 54-58, 60-66) differed significantly, so it was impossible to compare 'apples with oranges' in these cases. Unfortunately, the facility for high-temperature oxidation used in the present study (described in detail in (Ref 37)) did not enable to estimate both water and hydrogen concentrations in the test environments. However, based on the oxidation kinetics, the sample cross sections and the morphology of the oxide layers (Fig. 5, 6 and 8, respectively), it could be unambiguously concluded that steam played a significant role upon testing all investigated samples. Further research in this direction should be focused on a detailed study of the hydrogen content in the oxidized samples, similarly to (Ref 44), and variations in the microstructure of their oxide layers, applying up-to-date methods such as in situ neutron radiography (Ref 14) and neutron scattering (Ref 15).

5. Conclusions

The obtained results enabled to draw the following conclusions.

1. HIPIB irradiation led to more uniform surface reliefs on the samples from the Zr-1%Nb alloy. In particular, no initial shallow scratches were found while deeper discontinuities were characterized by smoother reliefs. Despite the presence of some typical craters, the *Ra* surface roughness decreased down to 50-60 nm, which was only half of the initial value of $\sim$ 100 nm. HIPIB irradiation did not change the phase composition of the Zr-1%Nb alloy, but both *a* and *c* lattice parameters decreased slightly with increasing microstrains in the surface layer.
2. After HCPEB processing, the general patterns of changes in the surface layers were similar to those after HIPIB irradiation, but microcracks were found in some areas.
3. During oxidation of the samples at 1200 °C, the weight gains were greater in air than in steam in all studied cases. Nevertheless, diffusion of oxygen and the formation of oxide layers occurred more slowly in the surface

layers modified with both types of charged particles. The main reason for this phenomenon was the radiation-induced distortion of their crystal lattices. After HIPIB irradiation, the weight gain curves were the lowest in both air and steam environments. After HCPEB processing, the slightly faster weight gain dynamics was caused by the presence of microcracks and greater residual stresses in the surface layers. This fact was associated with different physical processes that had occurred when the surfaces had been modified with ion and electron beams.

4. Further research direction should be focused on irradiation of zirconium alloys with inert ions, as well as more detailed examinations of thin structures and hydrogen contents in the surface layers using advanced experimental equipment.

Acknowledgments

The work was supported by the following funding sources. The surface layers were irradiated and investigated, as well as the data were processed and the manuscript was written according to the project No. 20-21-00025 of Russian Foundation for Basic Research and State Atomic Energy Corporation 'Rosatom.' The samples were oxidized according to the Ministry of Science and Higher Education of the Russian Federation, project No. FWRF-2024-0006. The SEM studies were performed according to the Government research assignment for ISPMS SB RAS, project No. FWRW-2021-0003.

References

1. R. Tewari, K.V. Mani Krishna, and S. Neogy, *Zirconium and its alloys: properties and characteristics, comprehensive nuclear materials*, Vol 7 Elsevier, Amsterdam, 2020, p 284-302
2. Nuclear fuel behaviour in loss-of-coolant accident (LOCA) conditions. State-of-the-art report, nuclear energy agency OECD, (2009) p. 373
3. Y. Fukaya, T. Hirasaki, K. Kumagai, T. Tatsuoka, K. Takamori, and S. Suzuki, Corrosion Mitigation Activities Performed After the Fukushima Daiichi Accident, *Corrosion*, 2018, **74**(5), p 577-587. https://doi.org/10.5006/2695
4. M. Negyesi, T. Chmela, T. Veselsky, J. Krejci, L. Novotny, A. Pribyl, O. Blahova, J. Burda, J. Siegl, and V. Vrtllkova, Assessment of Oxygen Diffusion Coefficients by Studying High-Temperature Oxidation Behaviour of Zr1Nb Fuel Cladding in the Temperature Range of 1100-1300 °C, *J. Nucl. Mater.*, 2015, **456**, p 211-219. https://doi.org/10.1016/j.jnucmat.2014.09.035
5. G. Jiang, D. Xu, W. Yang, L. Liu, Y. Zhi, and J. Yang, High-Temperature Corrosion of Zr-Nb Alloy for Nuclear Structural Materials, *Prog. Nucl. Energy*, 2022, **154**, 104490. https://doi.org/10.1016/j.pnucene.2022.104490
6. T.K. Sawarn, S. Banerjee, A. Samanta, B.N. Rath, and S. Kumar, Study of Oxide and a-Zr(O) Growth Kinetics from High Temperature Steam Oxidation of Zircaloy-4 Cladding, *J. Nucl. Mater.*, 2015, **467**, p 820-831. https://doi.org/10.1016/jjnucmat.2015.10.012
7. M. Kiraly, K. Kulacsy, Z. Hozer, E. Perez-Fero, and T. Novotny, High-Temperature Steam Oxidation Kinetics of the E110G Cladding Alloy, *J. Nucl. Mater.*, 2016, **475**, p 27-36. https://doi.org/10.1016/j.jnucmat.2016.03.007
8. C.M. Lee, Y.-K. Mok, and D.-S. Sohn, High-Temperature Steam Oxidation and Oxide Crack Effects of Zr-1Nb-1Sn-0.1Fe Fuel Cladding, *J. Nucl. Mater.*, 2017, **496**, p 343-352. https://doi.org/10.1016/j.jnucmat.2017.10.013
9. T. Kato, I. Takagi, K. Sakamoto, and M. Aomi, Hydrogen Diffusivity in Oxide Layers Formed in Zr Alloy in Air or Steam, *J. Nucl. Mater.*, 2017, **494**, p 79-86. https://doi.org/10.1016/j.jnucmat.2017.07.010
10. M. Steinbrueck, F.O. da Silva, and M. Grosse, Oxidation of Zircaloy-4 in Steam-Nitrogen Mixtures at 600-1200 °C, *J. Nucl. Mater.*, 2017, **490**, p 226-237. https://doi.org/10.1016/j.jnucmat.2017.04.034
11. J. Krejci, V. Vrtilkova, J. Kabatova, A. Pribyl, P. Gajdos, D. Rada, and J. Sustr, High-Temperature Oxidation of a Sponge-Based E110 Cladding Tube Material: Weight Gain and Reaction Layer Kinetics, *Nucl. Technol.*, 2018, **201**(1), p 52-65. https://doi.org/10.1080/00295450.2017.1389595
12. M. Steinbruck, S. Prestel, and U. Gerhards, High-Temperature Interaction of Oxygen-Preloaded Zr1Nb Alloy with Nitrogen, *Nucl. Eng. Technol.*, 2018, **50**, p 237-245. https://doi.org/10.1016/j.net.2017.12.017
13. Y. Yan, B.E. Garrison, M. Howell, and G.L. Bell, High-Temperature Oxidation Kinetics of Sponge-Based E110 Cladding Alloy, *J. Nucl. Mater.*, 2018, **499**, p 595-612. https://doi.org/10.1016/j.jnucmat.2017.10.067
14. M. Grosse, S. Pulvermacher, M. Steinbruck, and B. Schillinger, In-situ neutron radiography investigations of the reaction of Zircaloy-4 in steam, nitrogen/steam and air/steam atmospheres, *Phys. B*, 2018, **551**, p 244-248.
15. Y. Yan, S. Qian, B. Garrison, T. Smith, and P. Kim, Nondestructive Hydrogen Analysis of Steam-Oxidized Zircaloy-4 by Wide-Angle Neutron Scattering, *J. Nucl. Mater.*, 2018, **502**, p 191-200. https://doi.org/10.1016/j.jnucmat.2018.02.016
16. E.K. Barsy, K. Kulacsy, Z. Hozer, M. Horvath, Z. Kis, B. Maroti, I. Nagy, R. Nagy, T. Novotny, E. Perez-Fero, A. Pinter-Csordas, and L. Szentmiklosi, Post-Test Examinations on Zr-1%Nb Claddings After Ballooning and Burst, High-Temperature Oxidation and Secondary Hydriding, *J. Nucl. Mater.*, 2018, **508**, p 423-433. https://doi.org/10.1016/j.jnucmat.2018.05.072
17. R. Thieurmel, J. Besson, E. Pouillier, A. Parrot, A. Ambard, and A.-F. Gourgues-Lorenzon, Contribution to the Understanding of Brittle Fracture Conditions of Zirconium Alloy Fuel Cladding Tubes During LOCA Transient, *J. Nucl. Mater.*, 2019, **527**, 151815. https://doi.org/10.1016/j.jnucmat.2019.151815
18. G. Jiang, D. Xu, L. Liu, X. Ding, W. Kuang, and M. Wang, Oxidation of Typical Zr-1Nb Alloy in High-Temperature air Under 700-900 °C, *Corros. Sci.*, 2022, **209**, 110701. https://doi.org/10.1016/j.corsci.2022.110701
19. M. Gestin, M. Mermoux, O. Coindreau, C. Duriez, M. Pijolat, V. Peres, and L. Favergeon, Experimental Study of Oxidation in Oxygen, Nitrogen and Steam Mixtures at 850 °C of Pre-Oxidized Zircaloy-4, *J. Nucl. Mater.*, 2019, **519**, p 302-314. https://doi.org/10.1016/jjnucmat.2019.03.020
20. R. Guillou, M. Le Saux, E. Rouesne, D. Hamon, C. Toffolon-Masclet, D. Menut, J.C. Brachet, J.L. Bechade, and D. Thiaudiere, In-Situ Time-Resolved Study of Structural Evolutions in a Zirconium Alloy During High Temperature Oxidation and Cooling, *Mater Charact*, 2019, **158**, 109971. https://doi.org/10.1016/j.matchar.2019.109971
21. C. Duriez, O. Coindreau, M. Gestin, A. Kasperski, V. Peres, M. Pijolat, H. Buscail, C. Issartel, R. Rolland, and M. Mermoux, Zircaloy-4 High Temperature Oxidation in Atmospheres Representative of SFP-LOCA: INVESTIGATION of the Influence of a Low Temperature Pre-Oxidation Scale, *J. Nucl. Mater.*, 2019, **513**, p 152-174. https://doi.org/10.1016/jjnucmat.2018.10.019
22. G. Jiang, L. Liu, D. Xu, Y. Li, W. Kuang, and M. Wang, Waterside Corrosion of M5 Alloy in Lithiated/Borated and Supercritical Water: INFLUENCES of Aqueous Environments, *J. Supercrit. Fluids*, 2023, **193**, 105828. https://doi.org/10.1016/j.supflu.2022.105828
23. W. Zhao, T. Wei, J.J. Liao, P. Song, X. Peng, Z. Liao, Q. Peng, and X. He, High-Temperature Oxidation Behavior of Zr-4 and Zr-Sn-Nb Alloy in Different Oxidation Ambient, *J. Alloys Compd.*, 2021, **887**, 161396. https://doi.org/10.1016/j.jallcom.2021.161396
24. R.B. Rebak, *Accident-tolerant materials for light water reactor fuels*, Elsevier, Amsterdam, 2020
25. J. Ko, J.W. Kim, H.W. Min, Y. Kim, and Y.S. Yoon, Review of Manufacturing Technologies for Coated Accident Tolerant Fuel Cladding, *J. Nucl. Mater.*, 2022, **561**, 153562. https://doi.org/10.1016/j.jnucmat.2022.153562
26. M. Slobodyan, High-Energy Surface Processing of Zirconium Alloys for Fuel Claddings of Water-Cooled Nuclear Reactors, *Nucl. Eng. Des.*, 2021, **382**, 111364. https://doi.org/10.1016/j.nucengdes.2021.111364
27. B. Sartowska, J. Piekoszewski, L. Waliś, and M. Barlak, Surface Morphology of Unalloyed Steels Remelted with Intense Plasma Pulses,

J. Microsc., 2010, **237**, p 370-373. https://doi.org/10.1111/j.1365-2818.2009.03262.x

28. J. Piekoszewski, B. Sartowska, M. Barlak, P. Konarski, L. Dąbrowski, W. Starosta, L. Walis, Z. Werner, C. Pochrybniak, K. Bochenska, P. Stoch, and W. Szymczyk, Improvement of High Temperature Oxidation Resistance of AISI 316L Stainless Steel by Incorporation of Ce-La Elements Using Intense Pulsed Plasma Beams, *Surf. Coat. Technol.*, 2011, **206**(5), p 854-858. https://doi.org/10.1016/j.surfcoat.2011.03.104
29. X. Liu, X. Mei, J. Qiang, G.E. Remnev, and Y. Wang, Effects on Structure and Properties of $Zr_{55}Al_{10}Cu_{30}Ni_5$ Metallic Glass Irradiated by High Intensity Pulsed Ion Beam, *Appl. Surf. Sci.*, 2014, **313**, p 911-917. https://doi.org/10.1016/j.apsusc.2014.06.106
30. X. Ma, G. Zhang, G. Wang, G. Zhu, W. Zhou, J. Wang, and B. Sun, Surface Morphology, Microstructure and Properties of as-cast AZ31 Magnesium Alloy Irradiated by High Intensity Pulsed Ion Beams, *Appl. Surf. Sci.*, 2014, **311**, p 567-573. https://doi.org/10.1016/j.apsusc.2014.05.109
31. P. Li, Y. Zou and Z.P. Zhang, Influence of High-Intensity Pulsed Ion Beam Irradiation Energy on Magnesium Alloy Surface Modification, *Vacuum*, 2015, **117**, p 8-11. https://doi.org/10.1016/j.vacuum.2015.03.025
32. M.K. Lei, X.P. Zhu, Y.P. Li, and D.M. Guo, Significance of Surface Integrity on High-Performance Manufacturing by Surface Modification, *Int. J. Adv. Des. Manuf. Technol.*, 2016, **82**(9-12), p 1831-1842. https://doi.org/10.1007/s00170-015-7467-6
33. X. Mei, X. Zhang, X. Liu, and Y. Wang, Effect on Structure and Mechanical Property of Tungsten Irradiated by High Intensity Pulsed Ion Beam, *Nucl. Instrum. Methods Phys. Res Sect. B*, 2017, **406**, p 697-702. https://doi.org/10.1016/j.nimb.2017.03.117
34. X.G. Han, J.F. Lv, Y.Z. Chen, Y.C. Shan, and J.J. Xu, Influence of Irradiation Intensity on Corrosion Properties of Microarc Oxidation Film on AZ31 Magnesium Alloy with HIPIB, *Anti-Corros. Methods Mater.*, 2019, **66**(4), p 418-424. https://doi.org/10.1108/ACMM-10-2018-2007
35. R.A. Nazipov, R.I. Batalov, R.M. Bayazitov, H.A. Novikov, V.A. Shustov, and E.N. Dulov, High-Intensity Pulsed Ion Beam Treatment of Amorphous Iron-Based Metal Alloy, *J. Phys. Conf. Ser.*, 2020, **1588**(1), p 012039. https://doi.org/10.1088/1742-6596/1588/1/012039
36. H. Zou, L. Zhang, T. Guan, X. Zhang, G.E. Remnev, S.K. Pavlov, Y. Wang, and X. Mei, Effect on Mechanics Properties and Microstructure of Molybdenum by High Intensity Pulsed Ion Beam Irradiation, *Surf. Coat. Technol.*, 2020, **384**, 125333. https://doi.org/10.1016/j.surfcoat.2020.125333
37. M.S. Slobodyan, S.K. Pavlov, and G.E. Remnev, Corrosion and High-Temperature Steam Oxidation of E110 Alloy and its Laser Welds After Ion Irradiation, *Corros. Sci.*, 2019, **152**, p 60-74. https://doi.org/10.1016/j.corsci.2019.02.031
38. V. Tarbokov, M. Slobodyan, S. Pavlov, E. Smolyanskiy, V. Uglov, and G. Remnev, Changes in Adhesion of CrN Coatings on Zr-1%Nb Alloy Substrates Preliminary Irradiated with High-Intense Pulsed Ion Beams, *High Temp. Mater. Processes*, 2022, **26**(3), p 7-19. https://doi.org/10.1615/HighTempMatProc.2022043388
39. M.V. Zhidkov, M.Y. Gazizova, A.E. Ligachev, S.K. Pavlov, and G.E. Remnev, Structure and Corrosion Properties of Stainless Steel After High-Power Ion Beam Processing, *IOP Conf. Ser.: Mater. Sci. Eng.*, 2021, **1014**, p 012061. https://doi.org/10.1088/1757-899X/1014/1/012061
40. M. Slobodyan, K. Ivanov, M. Elkin, V. Klimenov, S. Pavlov, G. Remnev, I. Strelkova, and V. Tarbokov, Effect of High-Current Pulsed Electron Beam Processing of Zr-1%Nb Alloy on its Oxidation Kinetics at 1200 °C in Air and Steam, *Corrosion*, 2022, **78**(2), p 163-167. https://doi.org/10.5006/3942
41. Y.I. Isakova and A.I. Pushkarev, Visualization and Analysis of Pulsed Ion Beam Energy Density Profile with Infrared Imaging, *Infrared Phys. Technol.*, 2018, **89**, p 140-146. https://doi.org/10.1016/j.infrared.2017.12.008
42. V. Tarbokov, S. Pavlov, E. Smolyanskiy, V. Uglov, M. Slobodyan, and G. Remnev, Effect of Preliminary Irradiation of 321 Steel Substrates with High-Intense Pulsed Ion Beams on Scratch Test Results of Subsequently Deposited AlN Coatings, *Coatings*, 2021, **11**(10), p 1169. https://doi.org/10.3390/coatings11101169
43. M.S. Slobodyan, V.N. Kudiiarov, and A.M. Lider, Effect of Energy Parameters of Pulsed Laser Welding of Zr-1%Nb alloy on Metal Contamination with Gases and Properties of Welds, *J. Manuf. Processes*, 2019, **45**, p 472-490. https://doi.org/10.1016/j.jmapro.2019.06.025
44. S. Suman, M.K. Khan, M. Pathak, R.N. Singh, and J.K. Chakravartty, Hydrogen in Zircaloy: Mechanism and its Impacts, *Int. J. Hydrogen Energy*, 2015, **40**(17), p 5976-5994. https://doi.org/10.1016/j.ijhydene.2015.03.049
45. J. Bair, M.A. Zaeem, and M. Tonks, A review on Hydride Precipitation in Zirconium Alloys, *J. Nucl. Mater.*, 2015, **466**, p 12-20. https://doi.org/10.1016/jjnucmat.2015.07.014
46. A.T. Motta, L. Capolungo, L.-Q. Chen, M.N. Cinbiz, M.R. Daymond, D.A. Koss, E. Lacroix, G. Pastore, P.-C.A. Simon, M.R. Tonks, B.D. Wirth, and M.A. Zikry, Hydrogen in Zirconium Alloys: A Review, *J. Nucl. Mater.*, 2019, **518**, p 440-460. https://doi.org/10.1016/j.jnucmat.2019.02.042
47. H. Zhong, J. Zhang, J. Shen, G. Liang, S. Zhang, M. Xu, X. Yu, S. Yan, G.E. Remnev, and X. Le, Dynamic Mechanism of Crater Formation Induced by Inclusion During Intense Pulsed Ion Beam Irradiation, *Vacuum*, 2020, **179**, 109541. https://doi.org/10.1016/j.vacuum.2020.109541
48. J. Cai, Q. Guan, P. Lv, C. Zhang, and Y. Yin, Crater Formation on the Surface of Pure Metal and Alloy Irradiated by High Current Pulsed Electron Beam, *High Temp. Mater. Processes*, 2018, **37**(8), p 777-784. https://doi.org/10.1515/htmp-2017-0067
49. A. Khan, M. Rafique, N. Afzal, Z. Khaliq, and R. Ahmad, Structural Characterization of Zircaloy-4 Subjected to Helium Ions Irradiation of Variable Fluence, *Nucl. Mater. Energy*, 2019, **20**, 100690. https://doi.org/10.1016/j.nme.2019.100690
50. N. Afzal, M. Rafique, A. Abbasi, R. Ahmad, M. Saleem, and J.-M. Lee, Impact of Variable Energy Hydrogen Ions on Structural and Mechanical Properties of Zircaloy-4, *Phys. Scr.*, 2018, **93**(11), 115303. https://doi.org/10.1088/1402-4896/aae215
51. J.-L. Béchade, D. Menut, S. Doriot, S. Schlutig, and B. Sitaud, X-ray Diffraction Analysis of Secondary Phases in Zirconium Alloys Before and After Neutron Irradiation at the MARS Synchrotron Radiation Beamline, *J. Nucl. Mater.*, 2013, **437**(1-3), p 365-372. https://doi.org/10.1016/j.jnucmat.2013.02.020
52. V.I. Boiko, A.N. Valyaev, and A.D. Pogrebnyak, Metal Modification by High-Power Pulsed Particle Beams, *Phys.-Usp.*, 1999, **42**(11), p 1139-1166. https://doi.org/10.1070/PU1999v042n11ABEH000471
53. N. Birks, G.H. Meier, and F.S. Pettit, *Introduction to the high-temperature oxidation of metals*, 2nd ed. Cambridge University Press, New York, 2006, p 352
54. R. Rolland, H. Buscail, and C. Issartel, Influence of Water Vapour on the Zircaloy-4 Oxidation at 700 °C: Stress Determination by in situ X-ray Diffraction, *Oxid. Met.*, 2017, **87**, p 491-500. https://doi.org/10.1007/s11085-016-9709-x
55. M. Guerain, C. Duriez, J.L. Grosseau-Poussard, and M. Mermoux, Review of Stress Fields in Zirconium Alloys Corrosion Scales, *Corros. Sci.*, 2015, **95**, p 11-21. https://doi.org/10.1016/j.corsci.2015.03.004
56. B. Cox, Oxidation of zirconium and its alloys, *Advances in corrosion science and technology*. M.G. Fontana, R.W. Staehle Ed., Springer, Boston, 1976, p 173-391. https://doi.org/10.1007/978-1-4615-9062-0_3
57. J.T. Prater, E.L. Courtright, High-temperature oxidation of zircaloy-4 in steam and steam-hydrogen environments. Richland, Pacific Northwest Laboratory (1986), p. 31
58. P. Hofmann, S. Hagen, G. Schanz, A. Skokan, Chemical interactions of reactor core materials up to very high temperatures. Karlsruhe, Kernforschungszentrum Karlsruhe GmbH, (1989), p. 68
59. M. Negyesi, J. Burda, O. Blahova, S. Linhart, and V. Vrtilkova, The Influence of Hydrogen on Oxygen Distribution Inside Zry-4 Fuel Cladding, *J. Nucl. Mater.*, 2011, **416**, p 288-292. https://doi.org/10.1016/j.jnucmat.2011.06.013
60. K. Park, S. Yang, and K. Ho, The Effect of High Pressure Steam on the Oxidation of Low-Sn Zircaloy-4 at Temperatures Between 700 and 900 °C, *J. Nucl. Mater.*, 2012, **420**, p 39-48. https://doi.org/10.1016/j.jnucmat.2011.09.014
61. J.-M. Lee, D.-H. Kook, I.-J. Cho, and Y.-S. Kim, A Study on the Reaction of Zircaloy-4 Tube with Hydrogen/Steam Mixture, *J. Nucl. Mater.*, 2017, **491**, p 105-114. https://doi.org/10.1016/j.jnucmat.2017.05.004
62. M. Negyesi and M. Amaya, Oxidation Kinetics of Zry-4 Fuel Cladding in Mixed Steam-Air Atmospheres at Temperatures of 1273-1473 K, *J.*

Nucl. Sci. Technol., 2017, **54**(10), p 1143-1155. https://doi.org/10.1016/j.jnucmat.2017.05.004

63. T.K. Sawarn, S. Banerjee, S.S. Sheelvantra, J.L. Singh, and V. Bhasin, Study of Clad Ballooning and Rupture Behaviour of Indian PHWR Fuel Pins Under Transient Heating Condition in Steam Environment, *J. Nucl. Mater.*, 2017, **495**, p 332-342. https://doi.org/10.1016/jjnucmat.2017.08.008
64. Y. Yan, T.A. Burtseva, and M.C. Billone, High-Temperature Steam-Oxidation Behavior of Zr-1Nb Cladding Alloy E110, *J. Nucl. Mater.*, 2009, **393**, p 433-448. https://doi.org/10.1016/j.jnucmat.2009.06.029
65. M. Steinbruck, N. Ver, and M. Groβe, Oxidation of Advanced Zirconium Cladding Alloys in Steam at Temperatures in the Range of 600-1200 °C, *Oxid. Met.*, 2011, **76**, p 215-232. https://doi.org/10.1007/s11085-011-9249-3
66. S. Banerjee, T.K. Sawarn, V.D. Alur, B.N. Rath, S. Kaity, K.M. Pandit, S. Anantharaman, and D.N. Sah, High Temperature Steam Oxidation Study on Zr-2.5%Nb Pressure Tube Under Simulated LOCA Condition, *J. Nucl. Mater.*, 2013, **439**, p 258-267. https://doi.org/10.1016/jjnucmat.2012.09.027